Mon. Not. R. Astron. Soc. **366,** 1346–1356 (2006) doi:10.1111/j.1365-2966.2005.09914.x

Tracing the nature of dark energy with galaxy distribution

P. Solevi,[1,2⋆] R. Mainini,[1,2] S. A. Bonometto,[1,2] A. V. Macciò,[3⋆] A. Klypin[4] and S. Gottlöber[5]

[1]*Physics Department G. Occhialini, Università degli Studi di Milano–Bicocca, Piazza della Scienza 3, I20126 Milano, Italy*
[2]*INFN, Via Celoria 16, I20133, Milano, Italy*
[3]*Institute for Theoretical Physics, University of Zürich, Winterturstrasse 190, CH–8057 Zürich, Switzerland*
[4]*Astronomy Department, New Mexico State University, Box 30001, Department 4500, Las Cruces, NM 88003-0001, USA*
[5]*Astrophysikalisches Institut Potsdam, An der Sternwarte 16,14482 Potsdam, Germany*

Accepted 2005 November 23. Received 2005 November 22; in original form 2005 March 31

ABSTRACT

Dynamical dark energy (DE) is a viable alternative to the cosmological constant. Constructing tests to discriminate between Λ and dynamical DE models is difficult, however, because the differences are not large. In this paper we explore tests based on the galaxy mass function, the void probability function (VPF), and the number of galaxy clusters. At high z, the number density of clusters shows large differences between DE models, but geometrical factors reduce the differences substantially. We find that detecting a model dependence in the cluster redshift distribution is a significant challenge. We show that the galaxy redshift distribution is potentially a more sensitive characteristic. We do this by populating dark matter haloes in N-body simulations with *galaxies* using well-tested halo occupation distributions. We also estimate the VPF and find that samples with the same angular surface density of galaxies, in different models, exhibition almost model-independent VPF which therefore cannot be used as a test for DE. Once again, geometry and cosmic evolution compensate each other. By comparing VPFs for samples with fixed galaxy mass limits, we find measurable differences.

Key words: methods: analytical – methods: numerical – galaxies: clusters: general – cosmology: theory.

1 INTRODUCTION

High-redshift supernovae, anisotropies of the cosmic microwave background (CMB), and data on the large-scale distribution of galaxies (Riess et al. 1998; Perlmutter et al. 1999; Tegmark, Zaldarriaga & Hamilton 2001; De Bernardis et al. 2000; Hanany et al. 2000; Halverson et al. 2001; Spergel et al. 2003; Percival et al. 2002; Efstathiou et al. 2002) indicate that ∼70 per cent of the energy density in the Universe arises from a smooth component with largely negative pressure. This component is dubbed dark energy (DE). Recently, Macciò, Governato & Horellou (2005) presented further arguments in favour of DE based on the local (∼5 Mpc) Hubble flow of galaxies. The nature of DE is still open to debate. Candidates range from a positive cosmological constant Λ – yielding a ΛCDM cosmology – to models with a slowly evolving self-interacting scalar field ϕ (dynamical DE; Ratra & Peebles 1988; Wetterich 1988), to even more exotic physics of extra dimensions (e.g. Dvali & Turner 2003).

ΛCDM cosmologies are easy to study and fit most data. Unfortunately, to give a physical motivation to the value of Λ, we need a *fine-tuning* of vacuum energy at the end of the last phase transition. To rival the success of ΛCDM, models with different kinds of DE tend to make predictions very close to it, and therefore discriminatory tests on DE nature are not easy to devise. Until now, most tests based on large-scale structure have dealt with the evolution of the cluster distribution. Using Press–Schechter-type approximations (Press & Schechter 1974, PS hereafter; Sheth & Tormen 1999, 2002, hereafter ST; Jenkins et al. 2001), the expected dependence of the cluster mass function on DE nature has been extensively studied (see, for example, Wang & Steinhardt 1998; Haiman, Mohr & Holder 2000; Majumdar & Mohr 2004; Mainini, Macciò & Bonometto 2003a). The results were used to predict the redshift dependence of various observables, such as temperature (T) or photon counts (N). In Section 2, we compare the (virial) mass functions for different DEs. An important – and often overlooked – factor is the dependence of halo concentration c on the DE equation of state. For a given virial mass, the concentration varies with DE nature by up to 80 per cent, as shown by simulations (Klypin et al. 2003; Linder & Jenkins 2003; Kuhlen et al. 2005). The model dependence of c is so strong that it can be used as a possible discriminatory test for strong lensing measurements (Dolag et al. 2004; Macciò 2005).

This paper focuses on galactic $\sim 10^{12} h^{-1}$ $M_\odot$ scales, which are also interesting for testing models of DE. In order to make a

⋆E-mail: solevi@mib.infn.it (PS); andrea@pegasus.physik.unizh.ch (AVM)

prediction we first need to know how to generate a distribution of galaxies, not just dark matter haloes. There are various ways of doing this. We decided to use recent results on the halo occupation distribution (HOD): the probability of finding N galaxies in a halo of mass M. The HOD properties have been studied in detail (Seljak 2000; Benson 2001; Bullock, Wechsler & Somerville 2002; Zheng et al. 2002; Berlind & Weinberg 2002; Berlind et al. 2003; Magliocchetti & Porciani 2003; Yang, Mo & van den Bosch 2003; van den Bosch, Yang & Mo 2003). Numerical simulations, including gas dynamics (White, Hernquist & Springel 2001; Yoshikawa et al. 2001; Pearce et al. 2001; Nagamine et al. 2001; Berlind et al. 2003; Yang et al. 2004) and semi-analytical models of galaxy formation (Kauffmann, Nusser & Steinmetz 1997; Governato et al. 1998; Kauffmann et al. 1999a,b; Benson et al. 2000a,b; Sheth & Diaferio 2001; Somerville et al. 2001; Wechsler et al. 2001; Benson et al. 2003; Berlind et al. 2003), were used to find a law describing how haloes split in subhaloes hosting individual galaxies.

In this way, we formulate predictions on galaxy mass functions and their z-dependence. In order to compare predictions with data we then need to disentangle the evolution of the mass function from the evolution of the M/L ratio, because observations provide luminosities of galaxies while our estimates give us halo masses. In this respect, one of the aims of this work is to estimate how precisely the M/L evolution should be known in order to use data on galactic scales to test DE nature. Potentially, M/L evolution can be predicted using galactic evolution models (see, for example, Bressan, Chiosi & Fagotto 1994; Portinari, Sommer-Larsen & Tantalo 2004, and references therein). Such predictions can be compared with weak lensing results or satellite dynamics (Prada et al. 2003). The latter methods will provide estimates of virial M/L for samples of galaxies at different z. This is exactly what we need in order to test different models for DE. Here we find that, for some statistics, the expected signal, i.e. the difference between models, is rather large. Hence, there is hope of detecting DE effects in spite of uncertainties in M/L ratios. Certainly, if galactic evolution predictions and high-z M/L estimates are compared, one can hardly prescind from taking into account accurately the impact of DE nature.

We run a series of N-body simulations with different equations of state. In these models, the ratio $w = p_{\rm de}/\rho_{\rm de}$ of the DE pressure to the energy density varies with z according to field dynamics. The models considered here are the Ratra–Peebles (RP, Ratra & Peebles 1988) models, and the models with supergravity (SUGRA, Brax & Martin 1999; Brax & Martin 2000; Brax, Martin & Riazuelo 2000). Appendix A gives a short summary of these models. Each model is specified by an additional parameter – the energy scale Λ of the self-interacting potential of the scalar field. Here we take $\Lambda = 10^3$ GeV for both models. In RP (SUGRA), w shows slow (fast) variations with z.

The void probability function (VPF) is an obvious candidate for discriminating between models. Fluctuations grow differently in different models. So, one may expect some differences in VPF. We use galaxy distributions to estimate the VPF at different redshifts. Whilst measuring VPF in simulations is straightforward, mimicking observations is slightly more complicated because it requires corrections for geometrical effects and because the answer depends on a definition of galactic populations. At $z = 0$ no model dependence of the VPF is expected or found. Predictions at higher z depend on how galaxy samples are defined. In particular, we show that, if equal angular density samples are considered, VPF results are independent of the DE nature. On the other hand, if we select samples above a fixed galactic mass M, a significant signal is found, which can be useful for testing the DE nature.

The plan of the paper is as follows. In Section 2 we discuss how geometry and galactic evolution affect the redshift distributions of galaxies and clusters. In Sections 3 and 4 we discuss the simulations and prescriptions of populating haloes with galaxies. In Sections 5 and 6 results on redshift distributions and the VPF are given. Finally, Section 7 is devoted to discussing our results and future perspectives.

2 GEOMETRICAL AND EVOLUTIONARY FACTORS

Let us consider a set of objects whose mass function is $n(>M, z)$. In a spatially flat geometry, their number between z and $z + \Delta z$, in a unit solid angle, is given by

$$N(>M, z, \Delta z) = \int_z^{z+\Delta z} {\rm d}z'\, D(z')\, r^2(z')\, n(>M, z'), \qquad (1)$$

with $D(z) = {\rm d}r/{\rm d}z$. For flat models,

$$D(z) = \frac{c}{H_0}\sqrt{\frac{\Omega_{\rm m}(z)}{\Omega_{\rm m0}(1+z)^3}}, \quad r(z) = \int_0^z {\rm d}z'\, D(z'). \qquad (2)$$

Here, $\Omega_{\rm m}(z)$ is the matter density parameter at the redshift z. The Friedman equation can be written in the form

$$H^2(z) = \frac{8\pi}{3} G \frac{\rho_{\rm m0}(1+z)^3}{\Omega_{\rm m}(z)} = H_0^2 \frac{\Omega_{\rm m0}(1+z)^3}{\Omega_{\rm m}(z)}. \qquad (3)$$

Along the past light cone, $a\,{\rm d}r = -c\,{\rm d}t$. So, by dividing the two sides by ${\rm d}z = -{\rm d}a/a^2$, one finds that $a\,{\rm d}r/{\rm d}z = a^2 c\,{\rm d}t/{\rm d}a$. Accordingly, $D(z) = {\rm d}r/{\rm d}z = c/H(z)$ is derived from equation (3).

When w is a constant, a useful expression, namely

$$D^2(z) = (c/H_0)(1+z)^{-3}[\Omega_{\rm m0} + (1-\Omega_{\rm m0})(1+z)^{3w}]^{-1}, \qquad (4)$$

can be obtained, which allows one to see that the geometrical factors increase both when w decreases and when $\Omega_{\rm m0}$ decreases in models with $w < 0$.

An extension to dynamical DE can be performed either by using the interpolating expressions yielding $\Omega_{\rm m}\,(z)$, for RP and SUGRA models, provided by Mainini et al. (2003b), or, equivalently, through direct numerical integration. We obtain the geometrical factor $r^2(z)D(z)$ shown in the upper panel of Fig. 1.

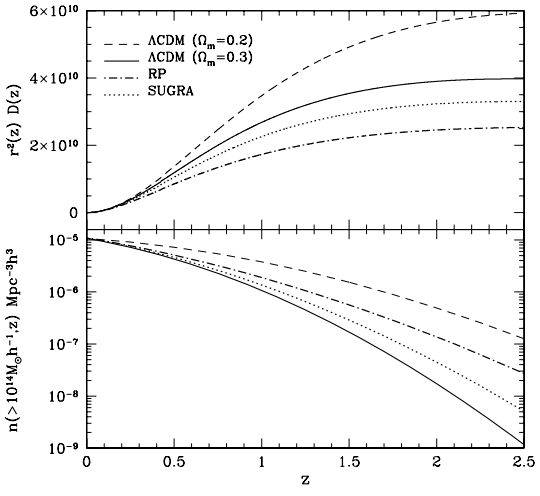

Figure 1. Geometrical and evolutionary terms on the cluster mass scale. In both panels, ΛCDM with $\Omega_{\rm m0} = 0.2$ is above ΛCDM with $\Omega_{\rm m0} = 0.3$. In contrast, in the upper and lower panels RP and SUGRA lie on opposite sides of ΛCDM. In the latter cases, cancellation between geometrical and evolutionary effects is therefore expected.

Here, $\Omega_{\rm m0} = 0.3$ or 0.2 for ΛCDM, while $\Omega_{\rm m0} = 0.3$ for SUGRA and RP models (for which $\Lambda = 10^3$ GeV). H_0 is 70 km s^{-1} Mpc^{-1} in all models ($h = 0.7$). In the absence of number density evolution, the upper panel of Fig. 1 shows the dependence of the angular number density on z.

In the PS formulation, the expected differential cluster number density $n(M)$, at a given time, is then given by the expression

$$f(\nu)\nu \mathrm{d}\log\nu = \frac{M}{\rho_{\rm m}} n(M) M \mathrm{d}\log M. \quad (5)$$

Here $\rho_{\rm m}$ is the matter density, $\nu = \delta_{\rm c}/\sigma_M$ is the *bias factor*, and M is the mass scale considered. σ_M is the rms density fluctuation on the scale M, and $\delta_{\rm c}$ is the amplitude that, in linear theory, fluctuations have in order that, assuming spherical evolution, full recollapse is attained exactly at the time considered (in a standard CDM model this value is ∼1.68; in other models, $\delta_{\rm c}$ is slightly different by a few per cent). As usual, we take a Gaussian $f(\nu)$ distribution.

Together with equation (5), we must take into account the virialization condition, which yields significantly different density contrasts $\Delta_{\rm v}$ in different DE models. Further details can be found in Mainini, Macciò & Bonometto (2003a).

In the lower panel of Fig. 1 we show the evolution of the number of haloes of mass $>10^{14}h^{-1}$ M$_\odot$ in comoving volumes. All models are normalized to the same cluster number today, and the redshift dependence of $n(>M, z)$ is clearly understandable on qualitative bases: when ΛCDM models are considered, the evolution is faster as we approach standard CDM. RP and SUGRA, however, yield a slower evolution than ΛCDM.

The important point is that, while both the geometrical factor and the evolutionary factor of ΛCDM (with $\Omega_{\rm m0} = 0.2$) lie above ΛCDM (with $\Omega_{\rm m0} = 0.3$), the RP and SUGRA factors lie on the opposite sides of ΛCDM.

When the two factors are put together, this causes the effect shown in the upper panel of Fig. 2: a strong signal on $\Omega_{\rm m0}$ and a widespread cancellation for DE models, compared with ΛCDM. Discriminating between different DE natures, from this starting point, is unavoidably a significant challenge.

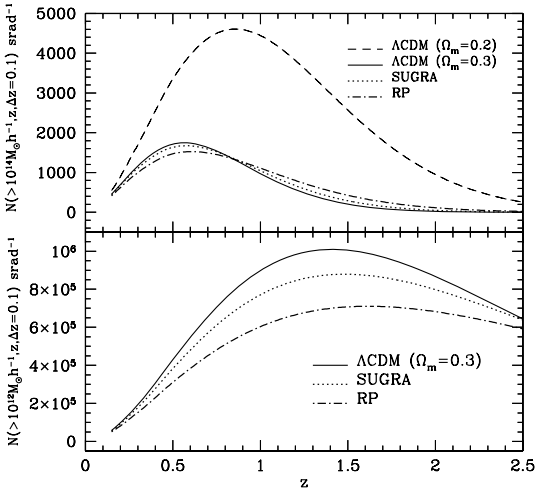

Figure 2. The upper panel shows how the redshift distribution on the cluster mass scale depends on the models. The cancellation expected from Fig. 1 has occurred and the models with $\Omega_{\rm m0} = 0.3$ are quite close, while ΛCDM allows large differences with varying $\Omega_{\rm m0}$. In the lower panel, similar curves are shown for haloes on galactic mass scales. In this case, evolution is almost model-independent and the geometrical factor causes an appreciable difference. On these scales, a lower $\Omega_{\rm m0}$ yields a different halo density, unless the spectrum is normalized to unphysical levels. Hence, only models with $\Omega_{\rm m0} = 0.3$ are shown.

Geometrical factors do not depend on the mass scale. On the contrary evolutionary factors are known to have a stronger dependence on the model for larger masses. As cancellation is almost complete on cluster scales, it is to be expected that geometrical factors yield a significant signal on lower mass scales. This is shown in the lower panel of Fig. 2, where haloes of $10^{12}h^{-1}$ M$_\odot$ are considered. A halo of this mass is expected to host a normal galaxy. More massive haloes are expected to host many galaxies. Hence, this plot cannot be directly compared with observations. Its main significance is that such lower mass scales deserve to be inspected because DE signals are expected to be strong enough on these scales.

3 SIMULATIONS

The simulations run for this work are based on a ΛCDM model and two dynamical DE models, with the same matter density and Hubble parameters ($\Omega_{\rm m0} = 0.3$ and $h = 0.7$). The simulations were run using the adaptive refinement tree code (ART; Kravtsov, Klypin & Khokhlov 1997). The ART code starts with a uniform grid, which covers the whole computational box. This grid defines the lowest (zeroth) level of resolution of the simulation. The standard particles–mesh algorithms are used to compute density and gravitational potential on the zeroth-level mesh. The ART code reaches high force resolution by refining all high-density regions using an automated refinement algorithm. The refinements are recursive: the refined regions can also be refined, each subsequent refinement having half of the cell size of the previous level. This creates a hierarchy of refinement meshes of different resolution, size, and geometry covering regions of interest. Because each individual cubic cell can be refined, the shape of the refinement mesh can be arbitrary and can match effectively the geometry of the region of interest.

The criterion for refinement is the local density of particles: if the number of particles in a mesh cell (as estimated by the cloud-in-cell method) exceeds the level $n_{\rm thresh}$, the cell is split ('refined') into eight cells in the next refinement level. The refinement threshold may depend on the refinement level. The code uses the expansion parameter a as the time variable. During the integration, spatial refinement is accompanied by temporal refinement. That is, each level of refinement, l, is integrated with its own time-step $\Delta a_l = \Delta a_0/2^l$, where Δa_0 is the global time-step of the zeroth refinement level. This variable time-stepping is very important for the accuracy of the results. As the force resolution increases, more steps are needed to integrate the trajectories accurately. Extensive tests of the code and comparisons with other numerical N-body codes can be found in Kravtsov et al. (1997) and Knebe et al. (2000).

The code was modified to handle DE of different types, according to the prescription of Mainini et al. (2003b). Modifications include effects arising from the change in the rate of the expansion of the Universe and from initial conditions, taking into account spatial fluctuations of the scalar field before they enter the horizon.

In this paper we use four new simulations. The models are normalized assuming $\sigma_8 = 0.9$. They are run in a box of $100\,h^{-1}$ Mpc. We use 256^3 particles with mass $m_{\rm p} = 4.971 \times 10^9\ h^{-1}$ M$_\odot$. The nominal force resolution is $3\,h^{-1}$ kpc. All models are spatially flat, while $\Omega_{\rm m0} = 0.3$ and $h = 0.7$. The two ΛCDM models start from different random numbers and are indicated as ΛCDM1 and ΛCDM2. The two DE models, named RP3 and SUGRA3, are started from the same random numbers as ΛCDM1.

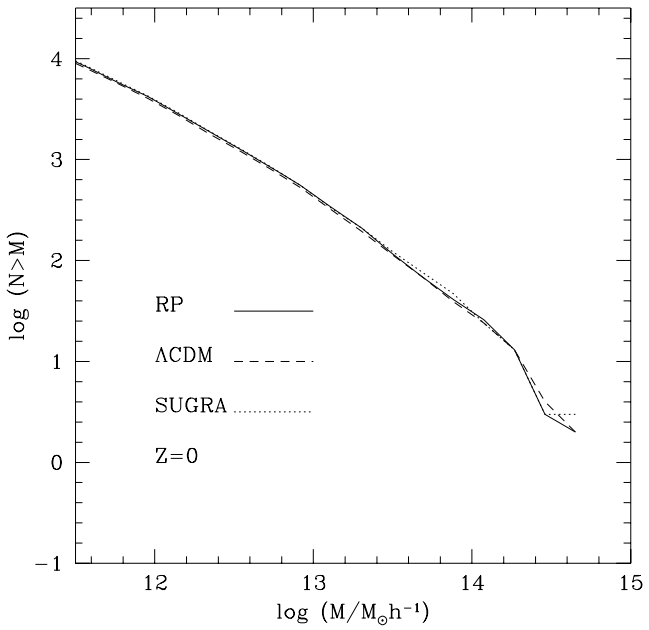

Figure 3. The halo mass function at $z = 0$. Results for Λ'3CDM (dashed line), RP (solid line), and SUGRA (dotted line) overlap.

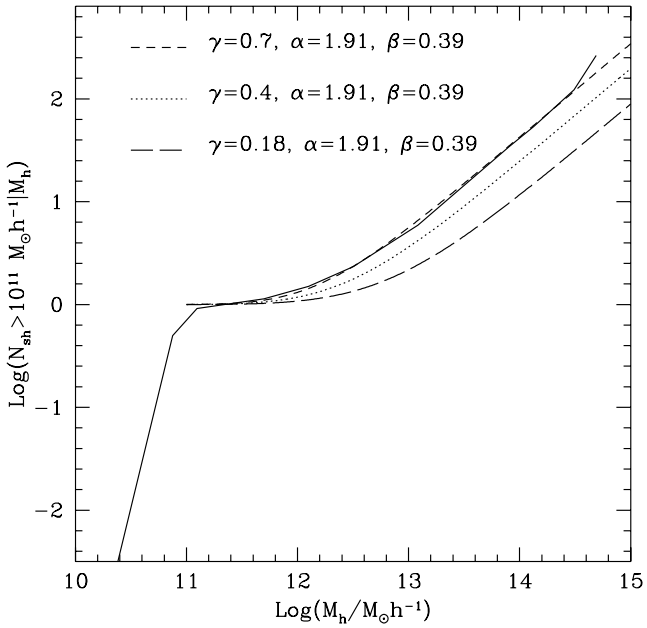

Figure 4. Comparison of different halo occupation distributions. The solid line is the halo occupation distribution given by Kravtsov et al. (2004). Other curves are obtained from equation (8) for various parameters γ as indicated in the plot.

4 GALAXIES IN HALOES

Haloes made by more than 30 particles were found in simulations by the spherical overdensity (SO) algorithm used in Klypin et al. (2003). The algorithm locates all non-overlapping largest spheres where the density contrast attains a given value Δ_v. Density contrasts are assigned the virialization values, which depend on the redshift z and on parameters of the DE. For instance, at $z = 0$, $\Delta_v = 101.0$ for ΛCDM, 119.4 for SUGRA3 and 140.1 for RP3; Δ_v values for higher z can be found in Mainini, Macciò & Bonometto (2003a; see also Mainini et al. 2003b).

Fig. 3 shows the halo mass function in the LCDM1, SUGRA3, and RP3 models at $z = 0$. Differences between the models result only from different $w(z)$, while their σ_8 is identical. Accordingly, at $z = 0$ their mass functions almost overlap and are well fitted by the Sheth–Tormen (ST, Sheth & Tormen 1999) approximation.

When we consider galaxies, however, we need to use another approach, because individual haloes may host many galaxies of different masses and luminosities. In order to assign galaxies to haloes we use a HOD. This is a relatively novel approach to locating galaxies in each halo. It can be used in a number of ways. Full-scale semi-analytical methods can predict quantities such as the luminosity, colours and star formation rates. Unfortunately, many important mechanisms are still poorly understood, making the results less reliable. It therefore seems advisable to minimize the physical input, leaving apart non-gravitational effects.

In this paper we use a prescription consistent with the results of Kravtsov et al. (2004). We utilize an analytical expression recently proposed by Vale & Ostriker (2004), but the parameters of the approximation are different from Vale & Ostriker (2004) and are tuned to produce a good fit to the results of Kravtsov et al. (2004). The approximation is based on the assumption that the probability $P_s(N_s|M)$ for a halo of mass M to host N_s subhaloes is approximately universal. We take the Schechter approximation

$$N(m|M)\,\mathrm{d}m = A\,\frac{\mathrm{d}m}{\beta M}\left(\frac{m}{\beta M}\right)^{-\alpha}\exp\left(-\frac{m}{\beta M}\right) \tag{6}$$

for the number of subhaloes with masses in the range m to $m + dm$, for a parent halo of mass M. A must be such that the total mass in subhaloes, $\int_0^\infty \mathrm{d}m\, mN(m|M)$, is a fraction γM of the parent halo mass. Therefore $A = \gamma/\beta\ \Gamma(2-\alpha)$, so that the number of subhaloes of mass m is

$$n_{sh}(m) = \int_0^\infty \mathrm{d}M\, N(m|M) n_h(M), \tag{7}$$

where $n_h\,(M)$ is the halo mass function, independently of the parent halo mass. The expression (6) yields the following number of subhaloes with mass $>m$ in a halo of mass M:

$$N_{sh}(>m, M) = \frac{\gamma}{\beta\Gamma(2-\alpha)}\int_{m/\beta M}^\infty \mathrm{d}x\, x^{-\alpha}\exp(-x). \tag{8}$$

Subhaloes will be then identified with galaxies. Fig. 4 shows that the expression approximates the results of Kravtsov et al. (2004) once we fit the parameters α, β, γ and add to the expression (8) a unity; that is, the halo as a subhalo of itself. For large haloes, to be interpreted as galaxy clusters, this subhalo could be the central cD, but adding an extra object, in such large galaxy sets, is just a marginal reset. For small haloes, on the other hand, it is important not to forget that they represent a galaxy, as soon as they exceed the galaxy mass threshold.

In a different context, Vale & Ostriker (2004) use the values $\gamma = 0.18$, $\beta = 0.39$. Owing to the use we make of equation (8), $\gamma = 0.7$ appears more adequate.

If the (differential) halo mass function $n_h(M)$ is known, the subhalo mass function is

$$N_{sh}(>m) = \frac{\gamma}{\beta\Gamma(2-\alpha)} \times \int_{m/\gamma}^\infty \mathrm{d}M\, n_h(M)\int_{m/\beta M}^\infty \mathrm{d}x\, x^{-\alpha}\exp(-x). \tag{9}$$

If we perform non-linear predictions, $n_h(M)$ is obtained from expression (5) or from the corresponding expressions in the ST case.

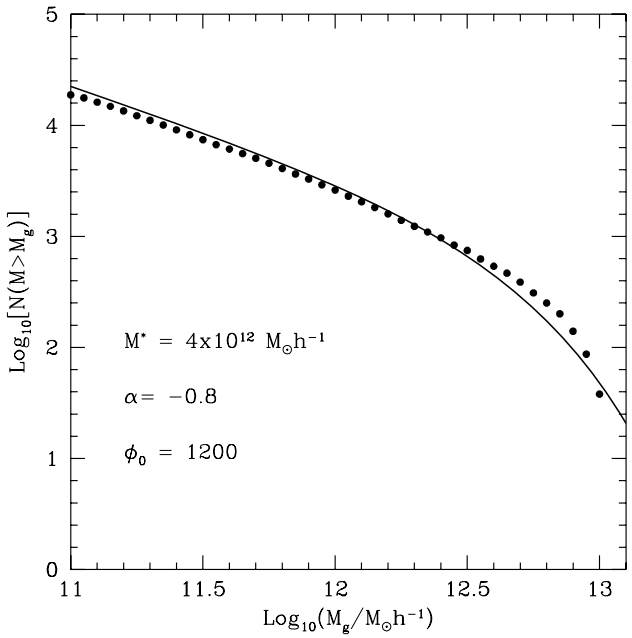

Figure 5. Galaxy (cumulative) mass function at $z = 0$ from simulations (dots) versus an integral Schechter function, with Φ_o, α and M_* shown in the frame.

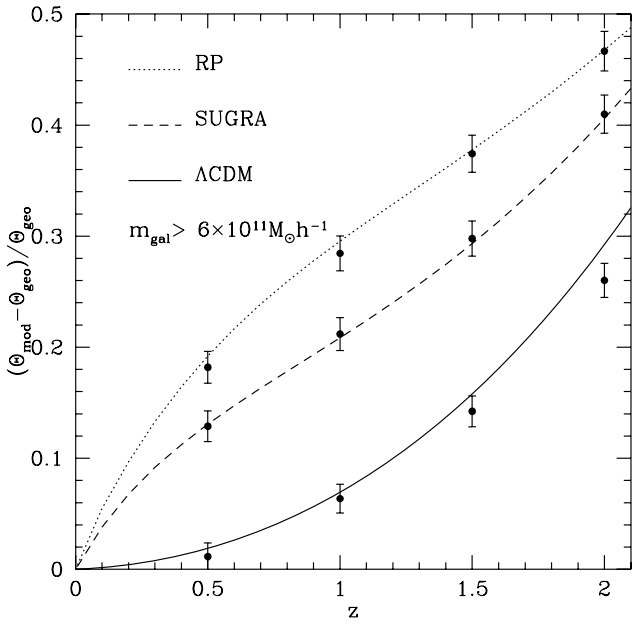

Figure 6. The redshift dependence of the mean fractional angular separation in different models. Points with error bars show the results of simulations. Curves indicate ST predictions. The plot shows a strong dependence of the galaxy redshift distribution on the dark energy nature.

When we deal with simulations, halo masses have discrete values $m_\nu = \nu m_{\rm p}$, appearing $n_{\rm h}^{(\nu)}$ times, up to a top mass $\nu_M m_{\rm p}$. Then

$$N_{\rm sh}(>m) = \frac{\gamma}{\beta\Gamma(2-\alpha)} \times \sum_{\nu=\frac{m}{\gamma m_{\rm p}}}^{\nu_M} n_{\rm h}^{(\nu)} \int_{\nu m/\beta M}^{\infty} {\rm d}x\, x^{-\alpha} \exp(-x). \quad (10)$$

In Fig. 5 we plot the galaxy mass function obtained with equation (10), using the mass function of haloes in the simulations, and identifying subhaloes with galaxies. At $z = 0$ model differences are indiscernible, and the plotted function holds for all models. We also plot a Schechter function with the parameters shown in the frame, selected to minimize the ratios between differential values at all points. As expected, the two curves are close. In fact, there must be some relation between masses and luminosities, but the $M_{\rm g}/L_{\rm g}$ ratio should not be a constant.

5 GALAXY ANGULAR DENSITY IN MODELS WITH DIFFERENT DARK ENERGY

Let us now consider the galaxy mass function at higher z, for the various models. According to equation (1), the number of galaxies with mass $>m$, in a solid angle $\Delta\theta^2(\Delta\theta \ll 1)$, between redshifts z and $z + \Delta z$, is

$$\frac{N_{\rm g}(>m, z; \Delta z, \Delta\theta)}{\Delta z \Delta\theta^2} \simeq c\,\frac{r^2(z)}{H(z)} n_{\rm g}(>m, z), \quad (11)$$

where $n_{\rm g}(>m, z)$ is the comoving number density of galaxies with mass $>m$ at a redshift z. The galaxy density can be obtained from the subhalo mass functions (9) and (10). Accordingly, the average angular distance $\theta_{\rm gg}$ is given by

$$\theta_{\rm gg}(>m, z)\sqrt{\Delta z} \simeq \frac{1}{r(z)} \left[\frac{H(z)}{n_{\rm g}(>m, z)}\right]^{1/2}. \quad (12)$$

Thus, the expression on the left-hand side is independent of the particular volume considered.

Such $\theta_{\rm gg}(>m, z)$ therefore depends on geometry, halo mass function and HOD. We expect, however, that the redshift dependence mostly arises from geometry, while evolution plays a significant role at higher z. In fact, the main difference between this and the cluster case is that evolution is mild and discrepancies between models, in comoving volumes, up to $z \sim 2$, are even weaker.

Let $\theta_\Lambda(z)$, $\theta_{\rm SU}(z)$ and $\theta_{\rm RP}(z)$ be the mean angular distances between galaxies at redshift z for the ΛCDM, SUGRA and RP models, respectively. Besides these functions, let us also consider the angular distance $\theta_{\rm geo}(z)$ obtained from equation (12), keeping the value of $n_{\rm g}(>m, z = 0)$ at any redshift and the ΛCDM geometry. Therefore, $\theta_{\rm geo}(z)$, although the symbol has no reference to ΛCDM, describes the behaviour of the angular separation *in a* ΛCDM model, in the limit of no halo evolution.

In Fig. 6, we compare results obtained from simulations with the ST predictions in different models. Rather than presenting $\theta_{\rm mod}(z)$ (where mod = λCDM, RP, SUGRA), we plot the fractional difference $(\theta_{\rm mod} - \theta_{\rm geo})/\theta_{\rm geo}$. In principle, error bars can be evaluated in two ways: (i) by comparing ΛCDM1 with ΛCDM2 (cosmic variance); and (ii) by comparing the differences between models. The latter evaluation can be done only at present because the models have the same power spectrum only at $z = 0$. The differences between models exist because the fluctuations grow differently in the past. At larger z, this *evolutionary variance* should be smaller, but is not easy to evaluate. We use differences between models at $z = 0$ as a rough estimate of error bars at all redshifts. Judging by the differences between ΛCDM1 and ΛCDM2, the cosmic variance seems to be smaller by a factor of 3 than the evolutionary differences. We find similar behaviour for different galaxy masses. In all cases, differences between models can be clearly seen.

The largest differences between models are attained at $z \sim 1$. Let us recall that the plot shows the fractional differences between DE models and the z-dependence due to the mere ΛCDM geometry.

At $z \simeq 1$, this difference is just $\simeq$5 per cent for ΛCDM, while for SUGRA it is ∼20 per cent, because of the different geometry and a still slower cosmological evolution. The difference with RP is even larger. This compares with an evolutionary variance hardly exceeding ∼2 per cent, if the effective comoving volume inspected is $\sim 10^6 h^{-3}$ Mpc^3. For $\Delta z \sim 0.1$, this corresponds to $\delta\theta \sim 30^\circ$–$40^\circ$.

The discriminating power of this theoretical prediction is to be compared with two possible sources of error: (i) peculiar velocities, setting individual galaxies into an apparent redshift band different from the one to which they belong; and (ii) luminosity evolution.

Overcoming the latter point is critical to the use of galaxies as indicators of DE nature, and we shall devote the whole of the next section to the impact of luminosity evolution. The conclusion of this discussion is that galaxies are indeed a possible indicator of DE nature, but more work is needed before they can be efficiently used for this purpose.

In this section we shall report the results of a test performed to evaluate the impact of redshift displacements resulting from peculiar velocities.

We divided the volume L^3 of the box into cells of side $10^{-1}\ L$, with volume $10^{-3}\ L^3$. 50 such cells were selected at random at each redshift and replaced by the cells at the closest redshift considered with their galaxy contents. The redshift displacement between the original cell and the replaced cell is ± 0.5. For a change of 5 per cent in galaxy contents, the average shift of $\theta_{\rm gg}$ is ∼1.2 per cent.

This shift lies well below the error bars shown in Fig. 6. However, the average errors resulting from evolutionary and cosmic variance plus peculiar velocities are ∼2.4 per cent, and the whole error never exceeds 2.6–2.7 per cent. We therefore argue that these sources of error do not affect the robustness of the results.

6 DEPENDENCE ON THE MASS–LUMINOSITY RELATION

Let us now consider galaxy evolution, which is expected to cause a z-dependence of the average $M_{\rm g}/L_{\rm g}$ ratio, but can also yield a z-dependence of the $M_{\rm g}/L_{\rm g}$ distribution about such an average, in a way that may depend on the mass range considered. From an observational point of view, when we consider galaxies of various luminosities $L_{\rm g}$, we must take into account that their expected mass $M_{\rm g}$ could be distributed with different laws at different z and $L_{\rm g}$.

Let us therefore consider the galaxy distribution on the $(M_{\rm g}, L_{\rm g})$-plane at a given z, yielding the galaxy number

$$\mathrm{d}N = D(M_{\rm g}, L_{\rm g}, [z])\, \mathrm{d}M_{\rm g}\, \mathrm{d}L_{\rm g} \tag{13}$$

in the infinitesimal area $\mathrm{d}M_{\rm g}\mathrm{d}L_{\rm g}$ about the point $(M_{\rm g}, L_{\rm g})$. We put z in brackets to emphasize that, in respect to it, D is not a *distribution* but a *function*. Obviously we expect a strong correlation between $M_{\rm g}$ and $L_{\rm g}$, at any z, so that it makes sense to consider an average $M_{\rm g}/L_{\rm g}$ ratio.

Once the distribution D is assigned, the distributions on $M_{\rm g}$(at fixed $L_{\rm g}$) and on $L_{\rm g}$(at fixed $M_{\rm g}$) read

$$\phi(M_{\rm g}, [z]) = \int \mathrm{d}L_{\rm g}\, D(M_{\rm g}, L_{\rm g}, [z]),$$

$$\psi(L_{\rm g}, [z]) = \int \mathrm{d}M_{\rm g}\, D(M_{\rm g}, L_{\rm g}, [z]).$$

The number $\mathrm{d}N$ is the product of $\phi(M_{\rm g}, [z])$ times the distribution on luminosities at fixed mass $M_{\rm g}$:

$$\mathrm{d}N = \phi(M_{\rm g}, [z])\, Q(L_{\rm g}; [M_{\rm g}, z])\, \mathrm{d}M_{\rm g}\, \mathrm{d}L_{\rm g}. \tag{14}$$

Equating the right-hand sides of equations (13) and (14) yields

$$Q(L_{\rm g}; [M_{\rm g}, z]) = \frac{D(M_{\rm g}, L_{\rm g}, [z])}{\int \mathrm{d}l\, D(M_{\rm g}, l, [z])}, \tag{15}$$

and, similarly, the distribution on masses at given $L_{\rm g}$ reads

$$P(M_{\rm g}; [L_{\rm g}, z]) = \frac{D(M_{\rm g}, L_{\rm g}, [z])}{\int \mathrm{d}m\, D(m, L_{\rm g}, [z])}. \tag{16}$$

We can now use P to work out the average $M_{\rm g}/L_{\rm g}$ at fixed $L_{\rm g}$, and the distribution on $M_{\rm g}/L_{\rm g}$ about such an average. Clearly,

$$\left\langle \frac{M_{\rm g}}{L_{\rm g}} \right\rangle_{L_{\rm g},z} = \frac{1}{L_{\rm g}} \int \mathrm{d}m\, m\, P(m; [L_{\rm g}, z]) = \\ = \frac{1}{L_{\rm g}} \frac{\int \mathrm{d}m\, m\, D(m, L_{\rm g}, [z])}{\int \mathrm{d}m\, D(m, L_{\rm g}, [z])}, \tag{17}$$

while the distribution

$$\mathcal{D}(M_{\rm g}; [L_{\rm g}, z]) = \frac{M_{\rm g}}{L_{\rm g}} \frac{D(M_{\rm g}, L_{\rm g}, [z])}{\int \mathrm{d}m\, D(m, L_{\rm g}, [z])} \tag{18}$$

tells us how $M_{\rm g}/L_{\rm g}$ is distributed around $\langle M_{\rm g}/L_{\rm g}\rangle_{L_{\rm g},z}$.

The impact of the evolution of stellar populations (or other mechanisms) on the $M_{\rm g}/L_{\rm g}$ ratio can be fully expressed through the distribution $D(M_{\rm g}, L_{\rm g}\,;[z])$ in equation (13). From it we can work out an average mass/luminosity ratio $\langle M_{\rm g}/L_{\rm g}\rangle$ and the distribution on masses $\mathcal{D}$; they both depend on $L_{\rm g}$ and z.

Let us now try to discover how such a variable $\mathcal{D}$ distribution affects our results, taking into account that we mostly ignore how such variations occur. Accordingly, we shall proceed as follows: we define a 'wild' distribution, which we expect to spread the $M_{\rm g}/L_{\rm g}$ ratio, at fixed $L_{\rm g}$, farther from average than any physical $\mathcal{D}$, at any z, will do. The effects caused by such a wild distribution should then be an overestimate of the effects of the actual distributions. Should they cause just a minor perturbation in estimates, all we have to worry about is the redshift dependence of the average $\langle M_{\rm g}/L_{\rm g}\rangle_{L_{\rm g}}$.

In more detail, we shall allow that a galaxy of given mass $M_{\rm g}$ has a luminosity in an interval L_1, L_2, with $L_2 \sim 20\, L_1$. We test this prescription without direct reference to luminosities: in the sample of galaxies obtained through the HOD, at each z, each galaxy mass (m) is replaced by a mass $m' = m + \Delta m\, R$, R being a random number with normal distribution and unit variance. We take $\Delta m = 0.8\, m$, but replace all $m' < 0.1\, m$ with $0.1\, m$, as well as all $m' > 1.9\, m$ with $1.9\, m$. The shift is therefore symmetric on m (not on log m). The operation causes a slight increase of the mass function above $\bar{M} \sim 2.8 \times 10^{11}\, h^{-1}\, \mathrm{M}_\odot$ (by a few per cent), as there are more lighter galaxies coming upwards than heavier galaxies going downwards [below $\bar{M}$, the low-mass cut-off of the mass function, set by the mass resolution of our simulations (see Section 3), begins to cause a shortage of transfers upwards]. The operation is then completed by reducing all masses by a (small) constant factor, so that, summing up all masses of objects with mass $M_{\rm g} > \bar{M}$, we have the same total mass as before the operation. This lowers the limit below which the mass function preserves its initial shape, but we never use galaxy samples including masses below $3 \times 10^{11} h^{-1}\, \mathrm{M}_\odot$.

We re-estimated $\theta_{\rm mod}\sqrt{\Delta z}$ using the new masses, for the same mass limits as before, and compared the changes obtained in this way with the Poisson uncertainty arising from the finite number of galaxies in each sample.

We find that the error obtained from the above procedure ranges between 20 and 40 per cent of the Poisson error.

This output tells us that the evolution of the physical distribution can be expected to redistribute results well inside the Poisson

uncertainty. If we expect this redistribution to be random, the top value of the whole expected error is then 3 per cent; if we attribute a systematic character to it and refrain from performing a quadratic sum with the other error sources considered, the overall possible error is still within 3.8 per cent. It should be emphasized that here we pushed all error sources to their maximum; thus, we believe that the above estimates are safely conservative.

Let us now discuss how the evolution of the average M_g/L_g ratio can affect the use of galaxies to detect DE nature. In principle, one could use the z-dependence of $D(M_g, L_g)$ to obtain the z-dependence of the $\langle M_g/L_g\rangle_{L_g}$ ratio. More realistically, suitable data sets can directly provide the z-dependence of $\langle M_g/L_g\rangle_{L_g}$, with some residual uncertainty. The basic issue is then: how well does the z evolution of $\langle M_g/L_g\rangle_{L_g}$ need to be known in order that DE nature can be tested? Fig. 6 is devised to provide a direct reply to this question: if we double the values of $\delta\,\theta_{gg}/\theta_{gg}$ provided there, we have a fair estimate of the difference between evolution rates of $\mathcal{R} = \langle M_g/L_g\rangle_{L_g}(z)/\langle M_g/L_g\rangle_{L_g}(z=0)$ needed just to cover the differences between geometry and dynamics for the ΛCDM model or to compensate the differences between the ΛCDM geometry and whole evolution for dynamical DE models (in the limit $M_g \ll M_*$, where M_* is the mass-scale appearing in a Schechter-like expression). Fig. 6 can be interpreted in both senses, by changing the name of the ordinate.

For instance, at $z = 0.5$, an uncertainty ∼20 per cent (35 per cent) on the evolution of M_g/L_g is needed to hide the difference between ΛCDM and SUGRA (RP).

Let us demonstrate this point. From equation (12), $\theta_{gg} \propto n_g^{-1/2}$, so that a shift $\delta\,\theta_{gg}$ in the observed angular distance arises from a shift

$$\frac{\delta n_g}{n_g} \simeq 2\frac{\delta\theta_{gg}}{\theta_{gg}} \tag{19}$$

in the galaxy number density

$$n_g(>M_g) = n_g\left(>L_g\frac{M_g}{L_g}\right). \tag{20}$$

The latter shift, as shown in equation (20), can arise from a shift on M_g/L_g, being

$$\delta n_g = n_g(M_g)L_g\,\delta\left(\frac{M_g}{L_g}\right); \tag{21}$$

here, $n_g(M_g)$ is the differential mass function, obtained by differentiating the integral mass function $n_g(>M_g)$. Therefore,

$$\frac{\delta n_g(>M_g)}{M_g n_g(M_g)} \simeq \frac{\delta(M_g/L_g)}{(M_g/L_g)} \tag{22}$$

and

$$\frac{\delta(M_g/L_g)}{(M_g/L_g)} \simeq \frac{\delta n_g(>M_g)}{n_g(>M_g)}\frac{n_g(>M_g)}{M_g n_g(M_g)}. \tag{23}$$

If we approximate the integral mass function by a Schechter expression, it is $|m\,n(m)/n(>m)| = 1 + m/M_*$, so that

$$\frac{\delta(M_g/L_g)}{(M_g/L_g)} \simeq \frac{\delta n_g(>M_g)}{n_g(>M_g)}\left(1+\frac{M_g}{M_*}\right)^{-1}. \tag{24}$$

Using this equation together with equations (19) and (23), we have the relation

$$\frac{\delta(M_g/L_g)}{(M_g/L_g)} \simeq 2\left(1+\frac{M_g}{M_*}\right)^{-1}\frac{\delta\theta_{gg}}{\theta_{gg}}, \tag{25}$$

telling us how to use Fig. 6 to estimate the evolution of M_g/L_g needed to yield the same effects as a change in DE nature. This equation also tells us how to use Fig. 6 for masses approaching M_*.

7 THE VOID PROBABILITY FUNCTION

Let us randomly throw spheres of radius R in a space where objects of various masses M are set. The probability $P_0(R)$ of finding no object with $M > M_{tr}$ in them, is the VPF for objects of mass $>M_{tr}$.

We expect and find no model dependence in the *galaxy* VPFs at $z = 0$. At $z > 0$, a critical issue is how M_{tr} is set. One can simply plan to determine the galaxy masses M_g from data (e.g. from L_g values), so to select galaxies with $M_g > M_{tr}$. As widely outlined, this choice involves several complications. Another option is to take the most *luminous* galaxies up to an average angular distance θ_{gg}.

Each threshold M_{tr}, for any z and Δz, yields a value of θ_{gg}. Fig. 6 shows how θ_{gg} depends on the model at a fixed threshold. Vice versa, if we keep, for that z and Δz, a fixed θ_{gg}, the relative M_{tr} varies with models. We can compare models either at fixed M_{tr} or at fixed θ_{gg}. Dealing with observations, the latter option is easier, but mixes up the intrinsic VPF dependence on the model and other features that also depend on the model.

Besides the threshold setting, another issue has a great operational relevance. In principle, VPFs can be evaluated in the comoving volumes where galaxies are set and compared there with VPFs from data. This is, however, inadequate to evaluate how discriminatory the VPF statistics are. To do so, we follow the following steps.

(i) From cartesian coordinates $\bar{x}_i (i = 1, 2, 3)$ in comoving volumes we work out the redshift and the celestial coordinates z, θ, ϕ that an observer, set at $z = 0$, would measure. This is achieved by using the geometry of the model.

(ii) Data also give z, θ, ϕ for each galaxy. To estimate the VPF, however, they must be translated into Cartesian coordinates x_i. An observer can only perform such a translation by using the geometry of a *fiducial* model, for example ΛCDM. The second step, to forge predictions, therefore amounts to re-transforming z, θ, ϕ into Cartesian coordinates x_i, but using now the *fiducial* ΛCDM geometry; x_is coincide with the $\bar{x}_i$s only for a ΛCDM cosmology. Let us call *fiducial* space the environment where galaxies are now set.

(iii) We then estimate the VPFs, for all models, in the fiducial space; these VPFs should be compared with observational data, but can also be compared with one another to assess how discriminatory these statistics can be.

Although comparing predictions for VPFs in comoving volumes, therefore, has little discriminatory meaning, our outputs are more easily explained if we start from comoving-space VPFs. Let us recall that, on galaxy scales, evolutionary differences up to $z \sim 2$ are modest. Accordingly, for an assigned M_{tr}, we find just marginal discrepancies, as is shown in Fig. 7 for $M_{tr} = 6 \times 10^{11}\ M_\odot\ h^{-1}$. Differences among VPFs arise, of course, if we do not fix M_{tr}, but θ_{gg}, as a reflex of θ_{gg} differences. These VPFs are shown in Fig. 8.

VPFs in respect of comoving coordinates bear a strict analogy with mass functions in comoving volumes. The fact that geometry erases almost any signal on the cluster mass function is analogous to what happens for the VPF when we pass from comoving to fiducial space. This fact is far from trivial. Let us compare these VPFs with the VPFs in a Poisson sample with the same θ_{gg} (Fig. 9) and recall that

$$P_0(R) = \exp\left[-\bar{N}_R + \sum_{n=2}^{\infty}\frac{(-\bar{N}_R)^n}{n!}\xi^{(n)}(R)\right]. \tag{26}$$

Here, $\bar{N}_R$ is the average number of points in a sphere of radius R; $\xi^{(n)}(R)$ are the n-point functions averaged within the same sphere. For the Poisson sample $P_0(R) = \exp(-\bar{N}_R)$, as all $\xi^{(n)}(R)$ vanish.

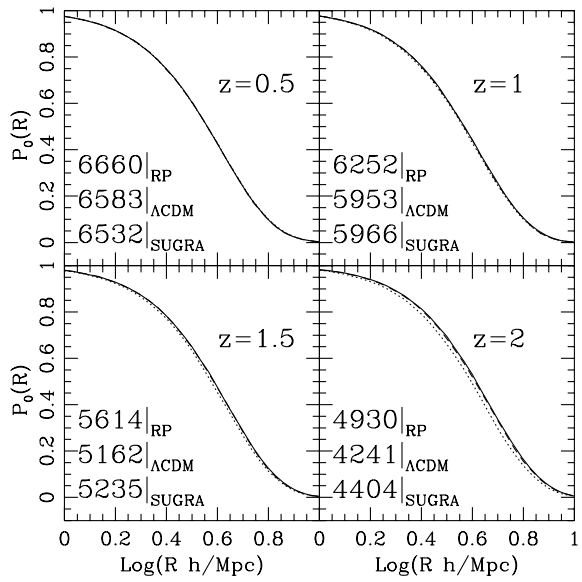

Figure 7. Void probability functions in comoving volumes for $M_{\rm tr} = 6 \times 10^{11}\,{\rm M}_{\odot}\,h^{-1}$. The four panels refer to redshifts 0.5, 1, 1.5 and 2, as indicated in the frames. The galaxy numbers in the simulation box are reported for each model. Solid, dashed and dotted lines as in Fig. 6.

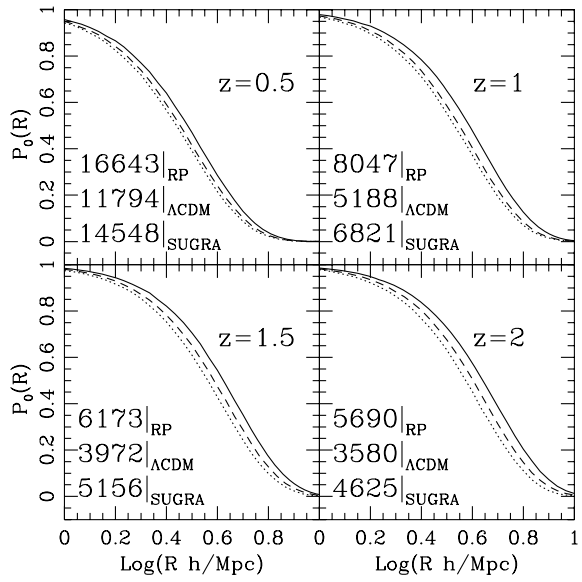

Figure 8. Void probability functions in comoving volumes for fixed angular density. The four panels refer to redshifts 0.5, 1, 1.5 and 2, as indicated in the frames. Numbers in the frames as in Fig. 7. Solid, dashed and dotted lines as in Fig. 6.

The difference between Poisson VPF and model VPF is to be fully ascribed to $\xi^{(n)}$, as $\bar{N}_R$ is set equal. This difference is huge, in respect of the differences between models, expected to arise because of $\xi^{(n)}$ shifts. The paucity of the shifts indicates that density renormalization almost erases the shifts in correlation functions of all orders.

The cancellation between geometrical and $\theta_{\rm gg}$ effects, shown in Fig. 10, indicates that the passage from comoving to fiducial coordinates bears a weight comparable with the differences shown in Fig. 8. It therefore comes as no surprise that VPFs, for fixed $M_{\rm tr}$, almost absent in the comoving space, are significant in the fiducial

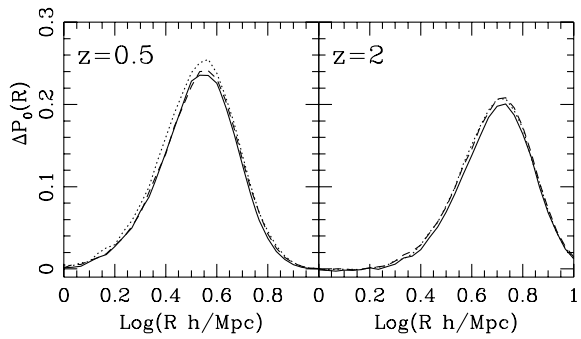

Figure 9. Differences between void probability functions of various models and the void probability function for a Poisson sample, in fiducial volumes for fixed angular density. They arise from the sum of n-point correlation functions in equation (26). Tiny residual differences between models, almost indiscernible in the previous plot, arise from differences between their n-point functions, clearly almost erased by geometrical renormalization.

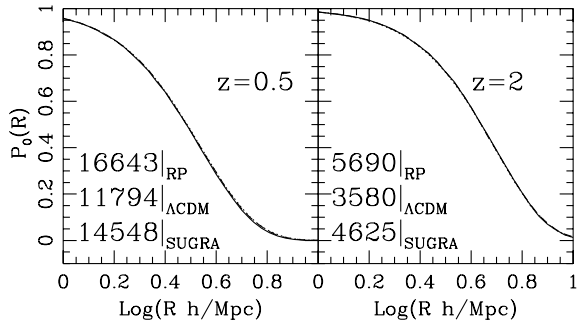

Figure 10. Void probability functions in fiducial volumes for fixed angular density. Numbers in the frames as in Fig. 7. Solid, dashed and dotted lines as in Fig. 6.

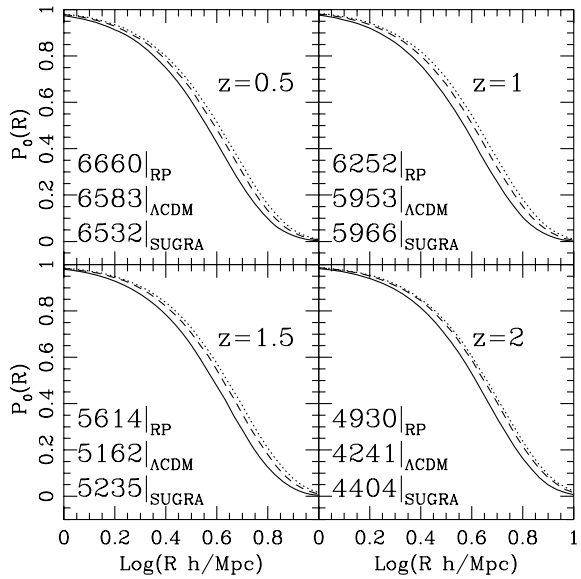

Figure 11. Void probability functions in fiducial volumes for a fixed mass limit (see text). Numbers in the frames as in Fig. 7. Solid, dashed and dotted lines as in Fig. 6.

space. They are shown in Fig. 11 and, as expected, the curves of the different models appear in the opposite order in respect to Fig. 8.

If the redshift dependence of the $M_{\rm g}/L_{\rm g}$ ratio is under control, Fig. 11 shows a discriminatory prediction that can be compared

with data. Once again, the problem concerns both the evolution of the mean M_g/L_g ratio and single galaxy deviations from average. Supposing that the average M_g/L_g evolution is under control, we can estimate the impact of individual deviations by replacing the sharp threshold on M_g with a soft threshold, substituting each galaxy mass M_g with $M_g + \Delta M_g\ R$, as in the previous section. This test was performed for samples as wide as those in our $100\,h^{-1}$ Mpc box, and the effects of such replacements are modest, amounting to $\sim$10 per cent of the difference found between ΛCDM and SUGRA.

Accordingly, the critical issue concerns the mean M_g/L_g ratio. By comparing VPFs for different thresholds, we can see that, in order that the shift of M_{tr} induces a VPF shift similar to differences between models, M_{tr} is to be displaced by a factor of 1.7–1.8. Uncertainties of $\sim$10 per cent on the mean M_g/L_g ratio would therefore leave intact the discriminatory power of the VPF statistics.

Before concluding this section, let us finally comment on sample variance. All ΛCDM VPFs were estimated on the ΛCDM1 simulation. Differences between ΛCDM1 and ΛCDM2 are, however, small, and could not be appreciated in the above plots. Accordingly, sample variance is not a relevant limit to the use of VPFs.

8 CONCLUSIONS

Dark energy modifies the rate of cosmic expansion in the epoch when a substantial fraction of fluctuations on cluster scales reach their turnaround. Therefore, it seems quite natural to trace the redshift dependence of $w(z) = p_{de}/\rho_{de}$ using the cluster mass function at different redshifts.

Unfortunately, the situation is more complicated. The evolution of $w(z)$ affects observations in two ways. First, it causes objects to form and evolve at different rates. Secondly, it results in a different mapping of comoving coordinates of galaxies to observed angular positions and redshifts. In conclusion on a cluster-mass scale ($\sim 10^{14} h^{-1}$ M$_\odot$), the evolutionary and geometrical effects tend to cancel, which makes clusters somewhat problematic for testing the equation of state.

In this paper we discuss the use of scales on which the evolutionary effects are minimized, so that the geometrical effects leave a clearer imprint. In a sense, this is not a new procedure: an analogous idea is utilized when the DE equation of state is tested by using a *standard candle*. Obviously, galaxies are not standard candles themselves, but they can provide a 'standard meter' through their (almost) model-independent abundance and evolution.

Previous analysis, which focused on clusters, tried to overcome the above difficulties by making recourse to various features. For example, the evolutionary dependence on w is preserved if one considers masses *well* above $10^{14} h^{-1}$ M$_\odot$. Unfortunately, clusters with masses $\sim 10^{15} h^{-1}$ M$_\odot$ or larger are rare today, and surely are even more rare in the past. Some analysis (see, for example, Haiman, Mohr & Holder 2000) stressed a possible role of very massive clusters at large z. However, the number of such clusters cannot be large, and thus comparing such predictions with observations is a significant challenge. There is also another problem with using cluster masses. Usually, the mass function is estimated with PS-like approximations, which are well tested with simulations. The 'virial' radius R_v is defined so that inside R_v the density contrast is Δ_v. The value of Δ_v depends on the redshift and on the DE model. On the other hand, data are typically analysed with a standard density contrast $\Delta_c \simeq 180$ (or 200). Increasing Δ_c reduces the amplitude of the mass function. If mass functions defined with variable Δ_v (almost) overlap one another, mass functions defined with constant Δ_c can be different. In order to account for these differences in the definitions, it is necessary to assume some shape for the density profile in the outskirts of clusters. This is typically done by using a Navarro, Frenk & White (NFW) profile with concentration $c_s \simeq 5$. As we deal with rather peripheral (virial) cluster regions, we can neglect the spread of actual values of concentration. However, when different $w(z)$ are considered, the *mean* c_s changes substantially, by up to 80 per cent (Klypin et al. 2003; Kuhlen et al. 2005). The differences between M_{200} and M_v are not large – 10 to 15 per cent. Approximately the same percentage of the difference depends on w. This may still be important. Neglecting these corrections may lead to substantial systematic errors.

As an alternative to using galaxy clusters, and so avoiding these and other problems, here we suggest exploiting the dependence on the DE nature of the redshift distribution of galaxies, and argue that the difficulties of this approach can be overcome.

A first problem is that it is necessary to know how to treat subhaloes of more massive haloes, because a large fraction of galaxies are hosted by subhaloes. To populate massive haloes with galaxies we use recent results on the HOD. Accordingly, we believe that this difficulty can be readily overcome.

Dealing with galaxies also requires knowledge of their masses M_g. The M_g–L_g relation is more complex than the relation between M_v, X-ray flux and T in clusters.

Galactic evolution studies and/or techniques aiming to compare dynamical or lensing masses with luminosities can be used for this purpose (Bressan et al. 1994; Portinari et al. 2004; Prada et al. 2003). It is also known that there is no one-to-one correspondence between L_g and M_g, as the luminosities of two galaxies of the same mass can be quite different, by up to one order of magnitude. We then considered two distinct issues. (i) How well must we know the evolution of $\langle M_g/L_g\rangle_{L_g}$? (ii) What could the impact be of fluctuations about such an average value, taking into account that the distribution about average can depend on z and mass?

How precisely $\langle M_g/L_g\rangle_{L_g}$ is to be known in order that different cosmologies can be safely discriminated is shown by Fig. 6. According to Section 6, if we double the values of $\delta\theta_{gg}/\theta_{gg}$ provided there, we have a fair estimate of the evolution rate $\mathcal{R} = \langle M_g/L_g\rangle_{L_g}(z)/\langle M_g/L_g\rangle_{L_g}(z=0)$ just covering the differences between models. Typically, if the estimated $\langle M_g/L_g\rangle_{L_g}$ evolution is reliable at a $\sim$10 per cent level, different models could be discriminated.

To reach this goal, fresh observational material is needed, but no conceptual difficulty is apparently involved in its acquisition.

The spread of the M_g/L_g ratio around its average value also must be treated carefully, as it could cause systematics. Here we reported the effect of a random spread of L_g in a luminosity interval L_1, L_2 with $L_2 \simeq 20\,L_1$. If the physical distribution of luminosities, for any mass and at any redshift, is within these limits, then possible systematics are well within errors arising from other effects.

Further tests on L_g spread were performed, but are not reported in detail in this paper. They apparently indicate that really wide and ad-hoc distributions are necessary, in order that possible systematics exceed the Poisson uncertainty.

Bearing these reservations in mind, we conclude that estimates of the redshift dependence of the average M_g/L_g, reliable within $\sim$10 per cent, can enable us to obtain reasonable information on DE nature.

In this paper we also discuss various tests based on the VPF. We find that the VPF is almost model-independent when estimated for samples with a constant angular number density of galaxies. This result apparently suggests that n-point functions are almost model-independent, at any z, once distances are suitably rescaled. If the

mean M_g/L_g is known, with a residual uncertainty not exceeding 10 per cent, we can also state that VPFs, for samples with a given M_{tr}, allow us to put in evidence the geometrical differences between models and are, therefore, a discriminatory statistic.

Combining the simulated halo distribution with the HOD provides an effective tool for testing the equation of state of DE. More work is needed to define the L_g–M_g relationship and, possibly, to reduce systematic effects. It is justifiable to expect that the z-dependence of the galaxy distribution, in deep galaxy samples, will allow us to constrain the DE nature even more reliably than the density of galaxy clusters in future compilations, sampling them up to large zs.

ACKNOWLEDGMENTS

We thank Loris Colombo and Cesare Chiosi for stimulating discussions. An anonymous referee is also to be thanked for improving the arguments now in Section 6. AK acknowledges financial support from NSF and NASA grants to NMSU. SG acknowledges financial support from DAAD. Our simulations were carried out at the LRZ computer center in Munich, Germany.

REFERENCES

Benson A. J., 2001, MNRAS, 325, 1039
Benson A. J., Baugh C. M., Cole S., Frenk C. S., Lacey C. G., 2000a, MNRAS, 316, 107
Benson A. J., Cole S., Frenk C. S., Baugh C. M., Lacey C. G., 2000b, MNRAS, 311, 793
Benson A. J., Frenk C. S., Baugh C. M., Cole S., Lacey C. G., 2003, MNRAS, 343, 679
Berlind A. A., Weinberg D. H., 2002, ApJ, 575, 587
Berlind A. A. et al., 2003, ApJ, 593, 1
Brax P., Martin J., 1999, Phys. Lett., B468, 40
Brax P., Martin J., 2000, Phys. Rev. D, 61, 103502
Brax P., Martin J., Riazuelo A., 2000, Phys. Rev. D, 62, 103505
Bressan A., Chiosi C., Fagotto F., 1994, ApJS, 94, 63
Bullock J. S., Wechsler R. H., Somerville R. S., 2002, MNRAS, 329, 246
De Bernardis P. et al., 2000, Nat, 404, 955
Dolag K., Bartelmann M., Perrotta F., Baccigalupi C., Moscardini L., Meneghetti M., Tormen G., 2004, A&A, 416, 853
Dvali G., Turner M., 2003, astro-ph/0301510
Efstathiou G. et al., 2002, MNRAS, 330, 29
Governato F., Baugh C. M., Frenk C. S., Cole S., Lacey C. G., Quinn T., Stadel J., 1998, Nat, 392, 359
Haiman Z., Mohr J. J., Holder G. P., 2000, ApJ, 553, 545
Halverson N. W. et al., 2001, ApJ, 568, 38
Hanany S. et al., 2000, ApJ, 545, L5
Huterer D., White M., 2002, ApJ, 578, L95
Jenkins A., Frenk C. S., White S. D. M., Colberg J. M., Cole S., Evrard A. E., Couchman H. M. P., Yoshida N., 2001, MNRAS, 321, 372
Kauffmann G., Nusser A., Steinmetz M., 1997, MNRAS, 286, 795
Kauffmann G., Colberg J. M., Diaferio A., White S. D. M., 1999a, MNRAS, 303, 188
Kauffmann G., Colberg J. M., Diaferio A., White S. D. M., 1999b, MNRAS, 307, 529
Klypin A., Macciò A. V., Mainini R., Bonometto S. A., 2003, ApJ, 599, 31
Knebe A., Kravtsov A. V., Gottloeber S., Klypin A., 2000, MNRAS, 317, 630
Kravtsov A., Klypin A., Khokhlov A., 1997, ApJS, 111, 73
Kravtsov A. V., Berlind A. A., Wechsler R. H., Klypin A. A., Gottlöber A., Allgood B., Primack J. R., 2004, ApJ, 609, 35
Kuhlen M., Strigari L. E., Zentner A. R., Bullock J. S., Primack J. R., 2005, MNRAS, 357, 387
Linder E. V., Jenkins A., 2003, MNRAS, 346, 573
Macciò A. V., 2005, MNRAS, 361, 1250
Macciò A. V., Governato F., Horellou C., 2005, MNRAS, 359, 941
Magliocchetti M., Porciani C., 2003, MNRAS, 346, 186
Mainini R., Macciò A. V., Bonometto S. A., 2003a, New Aston., 8, 173
Mainini R., Macciò A. V., Bonometto S. A., Klypin A., 2003b, ApJ, 599, 24
Majumdar S., Mohr J. J., 2004, ApJ, 613, 41
Nagamine K., Fukugita M., Cen R., Ostriker J. P., 2001, ApJ, 558, 497
Pearce F. R., Jenkins A., Frenk C. S., White S. D. M., Thomas P. A., Couchman H. M. P., Peacock J. A., Efstathiou G., 2001, MNRAS, 326, 649
Percival W. J. et al., 2002, MNRAS, 337, 1068
Perlmutter S. et al., 1999, ApJ, 517, 565
Portinari L., Sommer-Larsen J., Tantalo R., 2004, MNRAS, 347, 691
Prada F. et al., 2003, ApJ, 598, 260
Press W. H., Schechter P., 1974, ApJ, 187, 425
Ratra B., Peebles P. J. E., 1988, Phys. Rev. D, 37, 3406
Riess A. G. et al., 1998, AJ, 116, 1009
Seljak U., 2000, MNRAS, 318, 203
Sheth R. K., Diaferio A., 2001, MNRAS, 322, 901
Sheth R. K., Tormen G., 1999, MNRAS, 308, 119
Sheth R. K., Tormen G., 2002, MNRAS, 329, 61
Somerville R. S., Lemson G., Sigad Y., Dekel A., Kauffmann G., White S. D. M., 2001, MNRAS, 320, 289
Spergel D. N. et al., 2003, ApJS, 148, 175
Tegmark M., Zaldarriaga M., Hamilton A. J., 2001, Phys. Rev. D, 63, 43007
Vale A., Ostriker J. P., 2004, MNRAS, 353, 189
van den Bosch F. C., Yang X. H., Mo H. J., 2003, MNRAS, 340, 771
Wang L., Steinhardt P. J., 1998, ApJ, 508, 483
Wechsler R. H., Somerville R. S., Bullock J. S., Kolatt T. S., Primack J. R., Blumenthal G. R., Dekel A., 2001, ApJ, 554, 85
Wetterich C., 1988, Nucl. Phys. B, 302, 668
White M., Hernquist L., Springel V., 2001, ApJ, 550, L129
Yang X. H., Mo H. J., van den Bosch F. C., 2003, MNRAS, 339, 1057
Yang X. H., Mo H. J., Jing Y. P., van den Bosch F. C., Chu Y., 2004, MNRAS, 350, 1153
Yoshikawa K., Taruya A., Jing Y. P., Suto Y., 2001, ApJ, 558, 520
Zheng Z., Tinker J. L., Weinberg D. H., Berlind A. A., 2002, ApJ, 575, 617

APPENDIX A: DYNAMICAL DARK ENERGY MODELS

Dynamical DE is to be ascribed to a scalar field, ϕ, self-interacting through an effective potential $V(\phi)$, whose dynamics is set by the Lagrangian density:

$$\mathcal{L}_{DE} = -\frac{1}{2}\sqrt{-g}\left(\partial^\mu\phi\partial_\mu\phi + V(\phi)\right). \tag{A1}$$

Here, g is the determinant of the metric tensor $g_{\mu\nu} = a^2(\tau)\mathrm{d}x_\mu\mathrm{d}x_\nu$($\tau$ is the conformal time). In this work we need to consider just a spatially homogeneous ϕ ($\partial_i\phi \ll \dot{\phi}$; $i = 1, 2, 3$; dots denote differentiation with respect to τ). The equation of motion is then

$$\ddot{\phi} + 2\frac{\dot{a}}{a}\dot{\phi} + a^2\frac{\mathrm{d}V}{\mathrm{d}\phi} = 0. \tag{A2}$$

Energy density and pressure, obtained from the energy–momentum tensor $T_{\mu\nu}$, are

$$\rho = -T^0_0 = \frac{\dot{\phi}^2}{2a} + V(\phi),\ p = \frac{1}{3}T^i_i = \frac{\dot{\phi}^2}{2a} - V(\phi), \tag{A3}$$

so that the state parameter

$$w \equiv \frac{p}{\rho} = \frac{\dot{\phi}^2/2a - V(\phi)}{\dot{\phi}^2/2a + V(\phi)} \tag{A4}$$

changes with time and is negative as soon as the potential term $V(\phi)$ takes large enough values.

The evolution of dynamical DE depends on details of the effective potential $V(\phi)$. Here we use the model proposed by Ratra & Peebles (1988), which yields a rather slow evolution of w, and the model based on supergravity (Brax & Martin 1999, 2001; Brax & Martin 2000). The latter gives a much faster evolving w. The RP and SUGRA potentials

$$V(\phi) = \frac{\Lambda^{4+\alpha}}{\phi^{\alpha}} \qquad RP, \tag{A5}$$

$$V(\phi) = \frac{\Lambda^{4+\alpha}}{\phi^{\alpha}} \exp(4\pi G\phi^2) \qquad SUGRA \tag{A6}$$

cover a large spectrum of evolving w. These potentials allow tracker solutions, yielding the same low-z behaviour that is almost independent of initial conditions. In equations (A5) and (A6), Λ is an energy scale in the range 10^2–10^{10} GeV, relevant for the physics of fundamental interactions. The potentials depend also on the exponent α. Fixing Λ and α, the DE density parameter $\Omega_{\rm de,0}$ is determined. Here we use Λ and $\Omega_{\rm de,0}$ as independent parameters. In particular, numerical results are given for $\Lambda = 10^3$ GeV.

The RP model with such a Λ value is in slight disagreement with low-l multipoles of the CMB anisotropy spectrum data. Agreement may be recovered with smaller Λs, which, however, loose significance in particle physics. The SUGRA model considered here, on the other hand, is in reasonable agreement with all available data.

This paper has been typeset from a TEX/LATEX file prepared by the author.